Dynamic Modeling of miRNA-mediated Feed-Forward Loops

Federica Eduati[1], Barbara Di Camillo[1], Michael Karbiener[2], Marcel Scheideler[2], Davide Corà[3], Michele Caselle[4,5], Gianna Toffolo[1]

[1]*Department of Information Engineering, University of Padova, Padova, Italy;*

[2]*Institute for Genomics and Bioinformatics, Graz University of Technology, Graz, Austria;*

[3]*Institute for Cancer Research and Treatment (IRCC), School of Medicine, University of Torino, Torino, Italy;*

[4]*Department of Theoretical Physics, University of Torino and INFN, Torino, Italy;*

[5]*Center for Complex Systems in Molecular Biology and Medicine, University of Torino, Torino, Italy.*

Corresponding author:

Gianna Toffolo
University of Padova
Department of Information Engineering (DEI)
Via G. Gradenigo 6/B
35131 Padova
Italy
Tel: +39-049-8277804
FAX: +39-049-8277826

e-mail: toffolo@dei.unipd.it

CONTACT INORMATION

Federica Eduati

Department of Information Engineering, University of Padova, 35131 Padova, Italy
Phone: +39-049-8277640
e-mail: eduati@dei.unipd.it

Barbara Di Camillo

Department of Information Engineering, University of Padova, 35131 Padova, Italy
Phone: +39-049-8277671
e-mail: barbara.dicamillo@dei.unipd.it

Michael Karbiener

Institute for Genomics and Bioinformatics, Graz University of Technology, 8010 Graz, Austria
Phone: +43-316-873-5346
e-mail: michael.karbiener@tugraz.at

Marcel Scheideler

Institute for Genomics and Bioinformatics, Graz University of Technology, 8010 Graz, Austria
Phone: +43-316-873-5334
e-mail: marcel.scheideler@tugraz.at

Davide Corà

Institute for Cancer Research and Treatment (IRCC), School of Medicine, University of Torino, 10060 Candiolo, Torino, Italy
Phone: +39 011 9933241
e-mail: davide.cora@ircc.it

Michele Caselle

Department of Theoretical Physics, University of Torino and INFN, 10125 Torino, Italy
Center for Complex Systems in Molecular Biology and Medicine, University of Torino, 10125 Torino, Italy
Phone: +39- 011-6707205
e-mail: caselle@to.infn.it

Gianna Toffolo*

Department of Information Engineering, University of Padova, 35131 Padova, Italy
Phone: +39-049-8277804
e-mail: toffolo@dei.unipd.it

* Corresponding author

ABSTRACT

Given the important role of microRNAs (miRNAs) in genome-wide regulation of gene expression, increasing interest is devoted to mixed transcriptional and post-transcriptional regulatory networks analyzing the combinatorial effect of transcription factors (TFs) and miRNAs on target genes. In particular, miRNAs are known to be involved in feed-forward loops (FFLs) where a TF regulates a miRNA and they both regulate a target gene. Different algorithms have been proposed to identify miRNA targets, based on pairing between the 5' region of the miRNA and the 3'UTR of the target gene and correlation between miRNA host genes and target mRNA expression data.

Here we propose a quantitative approach integrating an existing method for mixed FFL identification based on sequence analysis with differential equation modeling approach that permits to select active FFLs based on their dynamics. Different models are assessed based on their ability to properly reproduce miRNA and mRNA expression data in terms of identification criteria, namely: goodness of fit, precision of the estimates and comparison with submodels. In comparison with standard approach based on correlation, our method improves in specificity.

As a case study, we applied our method to adipogenic differentiation gene expression data providing potential novel players in this regulatory network.

INTRODUCTION

MicroRNAs (miRNAs) are small (~ 22 nt) non-coding RNAs that post-transcriptionally regulate gene expression. They are transcribed as pri-miRNAs, then processed and exported from the nucleus to the cytoplasm in the form of pre-miRNA hairpins where they are cleaved by Dicer enzyme and incorporated in the RNA-induced silencing complex (RISC) to allow the interaction with target mRNAs via base pairing: binding to mRNA 3' UTR causes the decrease of the frequency of translation and the increase of mRNA degradation rate (Du and Zamore, 2005; Bartel, 2004; Baek, et al., 2008; Selbach, et al., 2008). MiRNAs are known to be involved in different biological processes, e.g. cell cycle control, cellular growth, differentiation, apoptosis and embryogenesis, and to play critical roles in human diseases (Jiang, et al., 2009). Their important regulatory role has come into focus in the last few years and main attention has been paid to miRNAs and their target genes identification (Lagos-Quintana, et al., 2003; Bentwich, et al., 2005; Jung, et al., 2010; Lagos-Quintana, et al., 2001). Different algorithms have been developed at this purpose, based on sequence data, looking for evolutionarily conserved Watson-Crick pairing between the 5' region of the miRNA and the 3'UTR of the target gene (Griffiths-Jones, et al., 2006; Bartel, 2009; Friedman, et al., 2009; Lewis, et al., 2003; Lewis, et al., 2005). There is also increasing interest in the dynamic description and the quantification of the regulation of gene expression by miRNAs and several scientific studies have characterized miRNA mediated degradation rates using models based on ordinary differential equation (Khanin and Vinciotti, 2008; Shimoni, et al., 2007; Levine, et al., 2007a; Levine, et al., 2007b; Vohradsky, et al., 2010).

Given the important role of miRNAs in genome-wide regulation of gene expression, increasing interest is devoted to mixed transcriptional and post-transcriptional regulatory networks analyzing the combinatorial effect of transcription factors (TFs) and miRNAs on target genes. In particular, miRNAs are known to be involved in feed-forward loops (FFLs) where a TF regulates a miRNA and

they both regulate a target gene (Shimoni, et al., 2007; Shalgi, et al., 2007; Tsang, et al., 2007; Re, et al., 2009). The dynamic of FFL has been extensively studied in transcriptional networks (Mangan and Alon, 2003; Kalir, et al., 2005; Kaplan, et al., 2008; Macia, et al., 2009; Alon, 2007) since this regulatory pattern is overrepresented in biological networks with respect to random networks (Milo, et al., 2002; Shen-Orr, et al., 2002) and thus represents a basic building block, favored by evolution and playing important functional roles. For example, FFLs involving miRNAs permit to accomplish target gene fine tuning and noise buffering (Li, et al., 2009; Wu, et al., 2009). In Tsang, et al. (2007) Correlation between miRNA host genes and target mRNA has been assessed together with conserved 3'UTR motifs to define putative regulatory relationships between a miRNA and a set of target genes sharing the same TF. A quantitative description of the regulatory interactions, e.g. based on differential equation models, could be helpful to characterize putative miRNA mediated FFLs. A similar approach has been adopted in (Vu and Vohradsky, 2007; Chen, et al., 2005; Chen, et al., 2004), where differential equations were fitted to expression data for transcriptional networks not involving miRNAs. As regards small RNA mediated FFL, a differential equation based model has been used in (Shimoni, et al., 2007) only to simulate the dynamic of a generic circuit using plausible parameter values derived from literature.

In this work we propose a general analytical framework based on the use of differential equations to extensively characterize a list of putative miRNA mediated FFLs. Our approach, when applied to a list of putative FFLs, provides some criteria to select active FFLs based on their ability to reproduce dynamic expression data. In this context, we do not use the data to validate the models, but, on the opposite, three models are used to fit the data and select active FFLs based on the goodness of fit. The first model M1 is borrowed from previous literature (Khanin and Vinciotti, 2008; Shimoni, et al., 2007; Levine, et al., 2007a; Levine, et al., 2007b). Models M2 and M3 are

linear simplifications of model M1 since, as shown in the following, the choice of the most appropriate model strictly depends on the available dataset.

We estimate the significance of our method in comparison with random FFLs obtained by randomly selecting links between miRNAs, TFs and target mRNA and in comparison with a more standard approach, based on correlation between TF, miRNA and target mRNA.

MODELS

In the miRNA mediated FFL circuit (Figure 1 A) a transcription factor TF (X_1) regulates a miRNA (X_2) and they both regulate a target mRNA (X_3). Three models based on ordinary differential equations (ODEs) are examined to describe the miRNA and target mRNA expression kinetics. All models consider X_1 as forcing function and describe the rate of change of X_2 and X_3 as the balance between their synthesis/transcription (S_i) and degradation (D_i) with the basal expression level (X_{ib}) as initial condition, the correspondent compartmental model is shown in Figure 1 B. Thus, for i=2,3, the differential equation describing the variables is

$$\dot{X}_i(t) = S_i(t) - D_i(t) \qquad X_i(0) = X_{ib} \tag{1}$$

The synthesis is expressed as the sum of a basal term (S_{ib}) plus a positive (activation) or negative (repression) term (ΔS_i) encoding the effect of the specific TF on the transcription of miRNA and target mRNA. As regards degradation (D_i), for miRNA it is assumed to be a function only of its expression while for the target mRNA the effect of the miRNA level is also modeled.

$$\dot{X}_2(t) = S_{2b} + \Delta S_2\left[X_1(t)\right] - D_2\left[X_2(t)\right]$$

$$\dot{X}_3(t) = S_{3b} + \Delta S_3\left[X_1(t)\right] - D_3\left[X_2(t), X_3(t)\right] \tag{2}$$

The three models adopt the same description for miRNA degradation, i.e. a first order process with constant rate d_2, while they differ in the functional description assumed for ΔS_2, ΔS_3 and D_3.

Model M1 describes the TF regulation on the miRNA (ΔS_2) and the target mRNA (ΔS_3) by a saturative Michaelis-Menten function, and the miRNA mediated degradation of the target mRNA (D_3) as the sum of a first order process, with constant rate, with respect to X_3 and a nonlinear

term that depends also on X_2 as in (Khanin and Vinciotti, 2008; Shimoni, et al., 2007; Levine, et al., 2007a; Levine, et al., 2007b).

Model M2 assumes TF regulation (ΔS_2, ΔS_3) to be linearly dependent on its level, while the functional description of target mRNA degradation (D_3) has nonlinear dynamics as in M1.

Model M3 is derived from M2 linearizing the miRNA mediated degradation model (D_3), thus the kinetics of the whole model is linear.

Since in log scale spot array data are expressed as differences with respect to a basal pre-differentiation state, it is convenient to consider as state variables $x_i = X_i - X_{ib}$ for i=1,2,3 where X_{ib} is the reference, collected at day -3. Considering that at the basal state $\dot{X}_i(t) = 0$ for i=2,3 it is possible to express the basal transcriptions S_i as function of the regulation parameters and the basal expression levels. After some passages, models M1, M2 and M3 turn out to be:

Model M1

$$\begin{aligned} \dot{x}_2(t) &= \frac{\alpha_2 x_1(t)}{\beta_2 + x_1(t)} - d_2 x_2(t) & x_2(0) &= 0 \\ \dot{x}_3(t) &= \frac{\alpha_3 x_1(t)}{\beta_3 + x_1(t)} - p x_3(t) - q x_2(t) - r x_2(t) x_3(t) & x_3(0) &= 0 \end{aligned} \qquad (3)$$

Model M2

$$\begin{aligned} \dot{x}_2(t) &= a_2 x_1(t) - d_2 x_2(t) & x_2(0) &= 0 \\ \dot{x}_3(t) &= a_3 x_1(t) - p x_3(t) - q x_2(t) - r x_2(t) x_3(t) & x_3(0) &= 0 \end{aligned} \qquad (4)$$

Model M3

$$\begin{aligned} \dot{x}_2(t) &= a_2 x_1(t) - d_2 x_2(t) & x_2(0) &= 0 \\ \dot{x}_3(t) &= a_3 x_1(t) - d_3 x_3(t) - s x_2(t) & x_3(0) &= 0 \end{aligned} \qquad (5)$$

The mathematical derivation of Equations 3, 4 and 5 and the meaning of each parameter in terms of synthesis and degradation rate are detailed in the Supplementary Material.

Model identification

A priori identifiability analysis of M1, M2 and M3 (Equations 3, 4 and 5) tested using the software DAISY (Bellu, et al., 2007), indicates that all three models are a priori globally identifiable, i.e. it is theoretically possible to estimate the set of unknown parameters $\boldsymbol{\theta}$ from the data, at least under ideal conditions (noise-free data, continuous time observations and error-free model structure).

$\hat{\boldsymbol{\theta}}$ can be estimated by Weighted Least Square, i.e. minimizing the Weighted Residual Sum of Squares (WRSS)

$$WRSS = \sum_{i=2,3}\sum_{j=1}^{N_i} \omega_i\left(t_j\right)\left[z_i\left(t_j\right) - x_i\left(t_j,\boldsymbol{\theta}\right)\right]^2 \tag{6}$$

where $z_i\left(t_j\right)$ is the observed datum at time j, $x_i\left(t_j,\boldsymbol{\theta}\right)$ is the predicted datum at time j computed using the model (Equations 3, 4 and 5), $\omega_i\left(t_j\right)$ is the weight assigned to datum j (inverse of the variance of the measurement error) and N_i is the number of time points. The external summation takes into account that residuals for both miRNA and target mRNA are simultaneously minimized, thus miRNA e mRNA time series collected under the same experimental conditions are required for model identification.

The measurement error is assumed to be Gaussian with zero mean and a known variance. The variance can be experimentally determined by analyzing replicates of each measure. A general model for the error variance is

$$v_i\left(t_j\right) = \alpha + \beta\left[z_i\left(t_j\right)\right]^{\gamma} \tag{7}$$

where α, β and γ are parameters to be estimated from replicates, e.g. by plotting the mean of each replicate against its variance and fitting on these data the unknown parameters of the error model (Equation 7), as described in (Cobelli, et al., 2000).

Since data are affected by a measurement error, also $\hat{\boldsymbol{\theta}}$ is affected by an error and the a posteriori identifiability of the models assesses the precision with which the parameters are estimated in terms of percentage coefficient of variation (CV)

$$CV\left(\hat{\boldsymbol{\theta}}\right) = \frac{SD\left(\hat{\boldsymbol{\theta}}\right)}{\hat{\boldsymbol{\theta}}} \cdot 100 \tag{8}$$

where $SD\left(\hat{\boldsymbol{\theta}}\right)$ is the standard deviation of the estimate.

FFLs selection

For each model, selection of active FFLs from a large set of putative ones exploits identification results in terms of consistency with the three following criteria:

1. *Goodness of fit.* A valid model should provide an adequate fit to the data. The goodness of fit can be evaluated on residuals, based both on their whiteness, i.e. residuals should be uncorrelated, and on their amplitude, i.e. deviation between predicted and observed values should be comparable to the measurement error. To evaluate the whiteness of the residuals, the number of runs, i.e. subsequences of residuals having the same sign, are analyzed for both miRNA and mRNA residual patterns. For the amplitude property, a global measure is provided by WRSS divided by the degree of freedom, i.e. difference between the number of data and the number of parameters: since weighted residuals should be independent with unit variance, WRSS should be the outcome of a random variable with Chi-Square distribution.

2. *Precision of the estimates.* FFLs having all parameters estimates with CV<100 are considered reliable.
3. *Comparison with submodels.* In order to verify that the FFL model (Figure 1 B) is the optimal description of the circuit, its performance is compared with that of two submodels (Figure 2) with missing regulatory links: in Submodel 1 the regulatory link between the TF and the target mRNA is missing, while in Submodel 2 the effect of miRNA on target mRNA degradation rate is not considered. Once the two submodels are identified, their performance is assessed versus the original one based on the Akaike Information Criterion (AIC) that implements the principle of parsimony, i.e. selects the model best able to fit the data with the minimum number of parameters:

$$AIC = WRSS + 2L \tag{9}$$

The FFL model is selected if its AIC is the lowest compared with submodels.

Summing up, if criteria 1 and 2 are satisfied for a dataset of putative FFL data, i.e. the model satisfactorily reproduces the data with all parameters precisely estimated from them, criteria 3 is applied and the FFL topology is finally selected as active provided that the complete model results to be the optimal model according to the AIC.

A CASE STUDY ON ADIPOGENESIS

To discuss a practical application of the proposed method, we applied it to miRNA and mRNA expression time series of human multipotent adipose-derived stem cells (hMADS) upon adipogenic differentiation. The initial panel of putative FFLs was selected based on sequence analysis; therefore it includes also false positive matches and/or FFLs non active during adipogenesis.

Data

Two independent cell culture experiments were performed as biological replicates during adipogenic differentiation of human mesenchymal stem cells as previously described in (Scheideler, et al., 2008; Karbiener, et al., 2009). Cells were harvested at the pre-confluent stage as reference (day -3) and at seven subsequent time points during human adipogenic differentiation: day -2 and 0 before, and 1, 2, 5, 10, 15 days after induction of differentiation. All hybridizations were repeated with reversed dye assignment (dye-swap). Background subtraction as well as global mean and dye swap normalization were applied. The resulting ratios were log2 transformed and the independent experiments were averaged. Complete miRNA and mRNA time-series expression data used for this study conform to the MIAME guidelines and are available in GEO database (GSE29186).

A list of mixed TF / miRNA FFLs was generated by means of a bioinformatic pipeline mainly based on an ab-initio sequence analysis of human and mouse regulatory regions as described in (Re, et al., 2009) using CircuitsDB (Friard, et al., 2010). Briefly, in CircuitsDB a catalogue of non-redundant promoter regions for protein-coding and miRNA genes in the human and mouse genomes were first constructed (see Supplementary Material for additional details). In parallel to that, a catalogue of non-redundant human and mouse 3'-UTR regions for protein-coding genes was defined. A transcriptional regulatory network and, separately, a list of post-transcriptionally

regulated genes was then generated for human by looking for conserved overrepresented motifs in the human and mouse promoters and 3'-UTRs previously assembled. The two networks were subsequently combined looking for mixed feed-forward regulatory loops, i.e. all the possible instances in which a master transcription factor regulates a miRNA and together with it a set of joint target coding genes.

Associating the list of 474 miRNA-mediated FFLs obtained using CircuitsDB with the available miRNA and mRNA time series data, the final dataset consisted of 329 putative FFLs (Supplementary Table S1) including 33 TFs, 35 miRNAs and 184 target mRNAs.

Measurement error

The measurement error models for miRNA and mRNA expression data were derived from the replicates, shown in Figure 3 A and B, respectively, as mean of the intensities versus their variance. To better define the dependence of the variance on the intensity, the positive x-axis was divided in intervals and, for each interval, the variance mean values were averaged as shown in Figure 3 C and D. By fitting Equation (7) on these data, the resulting models are

$$v_2\left(t_j\right) = 0.0484$$

$$v_i\left(t_j\right) = 0.033 + 0.031 \cdot z_i\left(t_j\right)^2 \qquad i = 1,3 \tag{10}$$

where v_2 and v_i in Equation (10) are referred to the miRNA and to the mRNA (valid for both TFs, and target mRNAs) datasets, respectively.

Implementation

To assess criterion 1, i.e. whiteness and amplitude of the residuals, statistical tests could not be applied due to the low number (seven) of samples. Thus, conservative empirical thresholds were

set to satisfy criterion 1: both miRNA and target mRNA residuals time series must have at least 3 runs and WRSS divided by the degree of freedom lower than 2. All computations were performed in the Matlab environment (Matlab R2010a), further details are supplied in the Supplementary Material.

Results

When the three criteria were applied to M1, no FFLs were selected as active, essentially because criterion 2 failed, indicating that the functional descriptions built in the model were too complex to be resolved from the available data. Conversely, 3 FFLs were selected with M2 and 23 with M3 as summarized in Table 1 and Table 2 respectively, where estimated parameters and their precision are reported. Two out of the three FFLs selected using M2 were identified also with M3, thus the total number of active FFLs is 24. It is interesting to notice that most of selected FFLs (21 out of 24) are incoherent. This type of FFL is known to play a significant role in biological regulation conferring precision and stability to gene expression regulation (Mangan and Alon, 2003; Wu, et al., 2009; Hornstein and Shomron, 2006; Osella, et al., 2011). As discussed in (Macia, et al., 2009), the target gene of incoherent FFLs generally shows a pulser response characterized by a rapid increase/decrease of its concentration followed by the return to a new basal level, while the target gene of coherent FFLs tends to exhibit a grader response characterized by a transient increase/decrease from the initial to the final state. These behaviors were confirmed by our data, as evident from Figure 4, where expression profiles of two incoherent (A) and two coherent (B) FFLs are shown along with the mean target gene expression levels (considering absolute values) between selected incoherent (C) and coherent (D) FFLs.

Analyzing the active FFLs from a biological point of view, it was found that out of the 24 selected FFLs, 9 FFLs involve TFs and 6 involve miRNAs (marked with an x in Table 1 and Table 2) that are

already known from the literature to be regulators of adipogenesis and adipocyte-related functions. A discussion of the results in comparison with the biological literature is available as Supplementary Material.

To estimate the significance of the proposed method, ten sets of 329 random FFLs were generated choosing one random miRNA and 2 random mRNA to play the role of the TF and the target gene respectively. Applying the previously described selection procedure, 0 FFLs were selected using M2 and an average of 15.6 FFLs, with a standard deviation of 1.5, were selected using M3. Instead, using a simple correlation analysis to choose FFLs having a correlation coefficient above 0.75 in absolute values for all three links, 12 FFLs were selected on the list of putative FFLs, and 18.6$\pm$4.6 were selected on the randomized datasets.

DISCUSSION

FFL selection procedure

In this work we propose a method to select active FFLs from a large set of putative ones based on miRNA and mRNA expression time series, using differential equation based models and identification criteria. A list of putative mixed transcriptional and post-trancriptional FFLs is generated on the basis of conserved overrepresented motifs in human and mouse promoters and 3' UTR. Identification of three alternative dynamic models, able to describe the miRNA and target mRNA dynamic data based on ordinary differential equations (ODEs) using the TF profile as forcing function, provides the basis for the selection of active FFLs. A putative FFL is selected as active if the feed-forward topology (Figure 1 A), associated with a plausible dynamic description, is necessary and sufficient to reproduce the available gene expression profiles, i.e. the model is able to reproduce data (criterion 1), outperforming with respect to submodels in terms of principle of parsimony (criterion 3) and its parameters can be estimated with acceptable precision from available data (criterion 2).

Comparison of dynamic models

Instead of postulating a univocal description for miRNA and mRNA expression kinetics, three models of increasing complexity are proposed. Model M1 assumes Michaelis-Menten kinetics for miRNA and target mRNA regulation accomplished by the TF and models miRNA mediated degradation of the target mRNA as a first order process with constant rate plus a nonlinear term dependent on miRNA and target mRNA expression. In model M2 linearity is assumed for TF regulation on miRNA and target mRNA, whereas nonlinearity is maintained for miRNA mediated degradation of the target mRNA. In M3 also the miRNA mediated degradation of the target mRNA is linearized, thus the whole model is described by a linear kinetics. The increasing complexity of

the models adapts to different type of gene expression data. The choice of the most appropriate model depends on the range and on the number of time points of the available time series and can be made using the same criteria described for the selection of active FFLs: goodness of fit, precision of the estimates and principle of parsimony. In particular, to estimate the Michaelis-Menten parameters of model M1 the whole Michaelis-Menten curve should be observable requiring expression data in an adequate range and sufficiently detailed. If these criteria are not satisfied by the available data, the linearization of the model still provide an adequate fit, allowing also a more precise estimation of the parameters. That does not mean that the more complex model is invalid, but only that the linearized one is more suitable for the available dataset.

Case study

In our case study, we used the three models on gene expression time series to select active FFLs during human adipogenesis. Since they showed a comparable ability to reproduce the data, the simplest model M3 was selected based on the principle of parsimony in 251 out of the 329 analyzed FFLs. Moreover, parameter estimates of model M1 were affected by very high CVs in all FFLs and those of M2 in all FFLs but 3, indicating that nonlinear models M1 and M2 were not a posteriori identifiable. Figure 5 shows the effect of the linearization of the synthesis mediated by the TF (ΔS_2), i.e. of using model M2 instead of M1 (panel A), and of the subsequent linearization of the degradation of the target mRNA (D_3), i.e. of using model M3 instead of M2 (panel B). In particular, using the analyzed dataset, the Michaelis-Menten curve is in the linear range (Figure 5 A left panel) and model M1 is not a posteriori identifiable (α_2 and β_2 show high CVs). In this case, X_1 is much lower than the half saturation constant β_2, then parameters α_2 and β_2 cannot be separately resolved but only the ratio between the two can be essentially estimated. Conversely, using M2 the parameter related to the synthesis mediated by the TF (ΔS_2) is a posteriori

identifiable (Figure 5 A right panel). Similarly, for the nonlinear description of the miRNA mediated degradation rate (Figure 5 B left panel) parameter r shows high CV and thus model M2 is not a posteriori identifiable. However, since rx_3 is much lower than q, the miRNA mediated degradation rate can be reasonably linearized as in M3 (Figure 5 B right panel) providing a simplification of the model with a reduced number of parameters and fit comparable to M2.

Analyzing the active FFLs from a biological point of view, it was found that out of the 24 selected FFLs, 9 FFLs involve TFs and 6 involve miRNAs (marked with an x in Table 1 and Table 2) that are already known from the literature to be regulators of adipogenesis and adipocyte-related functions. A discussion of the results in comparison with the biological literature is available as Supplementary Material; however, few information is available in the literature regarding miRNA mediated FFLs involved in adipogenesis and most datasets such the ones presented in (El Baroudi, et al., 2011) contain mainly information related to cancer. The limited available knowledge about human transcription networks and miRNA-mediated regulations in adipogenesis makes biological validation of regulatory links difficult and, at the same time, highlights the importance of the development of algorithms, like the one presented in this work, to predict testable regulation processes.

The significance of our method was estimated in comparison with random FFLs obtained by randomly selecting links between miRNAs, TFs and target mRNA. 329 random FFLs (equal to the number of putative FFLs estimated by pairing between the 5' region of the miRNA and the 3'UTR of the target gene) were generated ten times choosing one random miRNA and two random mRNAs to play the role of the TF and the target gene respectively. The previously described selection procedure was then applied to the randomized set of FFLs obtaining an average of 15.6 selected FFLs, with a standard deviation of 1.5. This can represent a rough estimation of the number of False Positive FFLs among the 24 selected by our method. Let's note that, if instead of

using differential equation based modeling, we select FFLs based on correlation between TF, miRNA and target mRNA, we select 12 FFLs on the original dataset and 18.6±4.6 on the randomized datasets, thus showing the increased specificity achieved by our approach.

The presented method selects triplets that can be explained by a simple FFL, whose effect can be isolated from the rest of the network, and described by one of the three proposed models. Thus, the presence of possible additional regulatory links is not excluded by our analysis, but we can say that, for the selected FFLs, this scheme provides a minimal plausible description of the regulatory interactions. The approach presented here does not allow identifying topologies incorporating more than one TF and/or miRNA. More complex topologies will be studied in future work by extending the approach here developed; moreover, we plan to analyze dynamic descriptions that will require a tighter sampling schedule.

ACKNOWLEDGMENTS

We thank Prof. Gérard Ailhaud, Dr. Christian Dani, and Dr. Ez-Zoubir Amri for hMADS cells.

AUTHOR DISCLOSURE STATEMENT

No competing financial interests exist.

REFERENCES

Alon, U. 2007. Network motifs: theory and experimental approaches. *Nat. Rev. Genet.* 8, 450-461.

Baek, D., Villen, J., Shin, C., et al. 2008. The impact of microRNAs on protein output. *Nature* 455, 64-71.

Bartel, D.P. 2009. MicroRNAs: target recognition and regulatory functions. *Cell* 136, 215-233.

Bartel, D.P. 2004. MicroRNAs: genomics, biogenesis, mechanism, and function. *Cell* 116, 281-297.

Bellu, G., Saccomani, M.P., Audoly, S., et al. 2007. DAISY: a new software tool to test global identifiability of biological and physiological systems. *Comput. Methods Programs Biomed.* 88, 52-61.

Bentwich, I., Avniel, A., Karov, Y., et al. 2005. Identification of hundreds of conserved and nonconserved human microRNAs. *Nat. Genet.* 37, 766-770.

Chen, H.C., Lee, H.C., Lin, T.Y., et al. 2004. Quantitative characterization of the transcriptional regulatory network in the yeast cell cycle. *Bioinformatics* 20, 1914-1927.

Chen, K.C., Wang, T.Y., Tseng, H.H., et al. 2005. A stochastic differential equation model for quantifying transcriptional regulatory network in Saccharomyces cerevisiae. *Bioinformatics* 21, 2883-2890.

Cobelli, C., Foster, D., and Toffolo, G. 2000. *Tracer kinetics in biomedical research: from data to model*. Kluwer Academic/Plenum, New York.

Du, T., and Zamore, P.D. 2005. microPrimer: the biogenesis and function of microRNA. *Development* 132, 4645-4652.

El Baroudi, M., Cora, D., Bosia, C., et al. 2011. A curated database of miRNA mediated feed-forward loops involving MYC as master regulator. *PLoS One* 6, e14742.

Fazi, F., Rosa, A., Fatica, A., et al. 2005. A minicircuitry comprised of microRNA-223 and transcription factors NFI-A and C/EBPalpha regulates human granulopoiesis. *Cell* 123, 819-831.

Friard, O., Re, A., Taverna, D., et al. 2010. CircuitsDB: a database of mixed microRNA/transcription factor feed-forward regulatory circuits in human and mouse. *BMC Bioinformatics* 11, 435.

Friedman, R.C., Farh, K.K., Burge, C.B., et al. 2009. Most mammalian mRNAs are conserved targets of microRNAs. *Genome Res.* 19, 92-105.

Griffiths-Jones, S., Grocock, R.J., van Dongen, S., et al. 2006. miRBase: microRNA sequences, targets and gene nomenclature. *Nucleic Acids Res.* 34, D140-4.

Hornstein, E., and Shomron, N. 2006. Canalization of development by microRNAs. *Nat. Genet.* 38 Suppl, S20-4.

Jiang, Q., Wang, Y., Hao, Y., et al. 2009. miR2Disease: a manually curated database for microRNA deregulation in human disease. *Nucleic Acids Res.* 37, D98-104.

Jung, C.H., Hansen, M.A., Makunin, I.V., et al. 2010. Identification of novel non-coding RNAs using profiles of short sequence reads from next generation sequencing data. *BMC Genomics* 11, 77.

Kalir, S., Mangan, S., and Alon, U. 2005. A coherent feed-forward loop with a SUM input function prolongs flagella expression in Escherichia coli. *Mol. Syst. Biol.* 1, 2005.0006.

Kaplan, S., Bren, A., Dekel, E., et al. 2008. The incoherent feed-forward loop can generate non-monotonic input functions for genes. *Mol. Syst. Biol.* 4, 203.

Karbiener, M., Fischer, C., Nowitsch, S., et al. 2009. microRNA miR-27b impairs human adipocyte differentiation and targets PPARgamma. *Biochem. Biophys. Res. Commun.* 390, 247-251.

Khanin, R., and Vinciotti, V. 2008. Computational modeling of post-transcriptional gene regulation by microRNAs. *J. Comput. Biol.* 15, 305-316.

Lagos-Quintana, M., Rauhut, R., Lendeckel, W., et al. 2001. Identification of novel genes coding for small expressed RNAs. *Science* 294, 853-858.

Lagos-Quintana, M., Rauhut, R., Meyer, J., et al. 2003. New microRNAs from mouse and human. *RNA* 9, 175-179.

Landgraf, P., Rusu, M., Sheridan, R., et al. 2007. A mammalian microRNA expression atlas based on small RNA library sequencing. *Cell* 129, 1401-1414.

Laneve, P., Gioia, U., Andriotto, A., et al. 2010. A minicircuitry involving REST and CREB controls miR-9-2 expression during human neuronal differentiation. *Nucleic Acids Res.* 38, 6895-6905.

Levine, E., Ben Jacob, E., and Levine, H. 2007a. Target-specific and global effectors in gene regulation by MicroRNA. *Biophys. J.* 93, L52-4.

Levine, E., Zhang, Z., Kuhlman, T., et al. 2007b. Quantitative characteristics of gene regulation by small RNA. *PLoS Biol.* 5, e229.

Lewis, B.P., Burge, C.B., and Bartel, D.P. 2005. Conserved seed pairing, often flanked by adenosines, indicates that thousands of human genes are microRNA targets. *Cell* 120, 15-20.

Lewis, B.P., Shih, I.H., Jones-Rhoades, M.W., et al. 2003. Prediction of mammalian microRNA targets. *Cell* 115, 787-798.

Li, X., Cassidy, J.J., Reinke, C.A., et al. 2009. A microRNA imparts robustness against environmental fluctuation during development. *Cell* 137, 273-282.

Macia, J., Widder, S., and Sole, R. 2009. Specialized or flexible feed-forward loop motifs: a question of topology. *BMC Syst. Biol.* 3, 84.

Mangan, S., and Alon, U. 2003. Structure and function of the feed-forward loop network motif. *Proc. Natl. Acad. Sci. U. S. A.* 100, 11980-11985.

Milo, R., Shen-Orr, S., Itzkovitz, S., et al. 2002. Network motifs: simple building blocks of complex networks. *Science* 298, 824-827.

Osella, M., Bosia, C., Corà, D., et al. 2011. The role of incoherent microRNA-mediated feedforward loops in noise buffering. *PLoS Comput. Biol.* 7, e1001101.

Re, A., Cora, D., Taverna, D., et al. 2009. Genome-wide survey of microRNA-transcription factor feed-forward regulatory circuits in human. *Mol. Biosyst* 5, 854-867.

Saini, H.K., Griffiths-Jones, S., and Enright, A.J. 2007. Genomic analysis of human microRNA transcripts. *Proc. Natl. Acad. Sci. U. S. A.* 104, 17719-17724.

Scheideler, M., Elabd, C., Zaragosi, L.E., et al. 2008. Comparative transcriptomics of human multipotent stem cells during adipogenesis and osteoblastogenesis. *BMC Genomics* 9, 340.

Selbach, M., Schwanhausser, B., Thierfelder, N., et al. 2008. Widespread changes in protein synthesis induced by microRNAs. *Nature* 455, 58-63.

Shalgi, R., Lieber, D., Oren, M., et al. 2007. Global and local architecture of the mammalian microRNA-transcription factor regulatory network. *PLoS Comput. Biol.* 3, e131.

Shen-Orr, S.S., Milo, R., Mangan, S., et al. 2002. Network motifs in the transcriptional regulation network of Escherichia coli. *Nat. Genet.* 31, 64-68.

Shimoni, Y., Friedlander, G., Hetzroni, G., et al. 2007. Regulation of gene expression by small non-coding RNAs: a quantitative view. *Mol. Syst. Biol.* 3, 138.

Tsang, J., Zhu, J., and van Oudenaarden, A. 2007. MicroRNA-mediated feedback and feedforward loops are recurrent network motifs in mammals. *Mol. Cell* 26, 753-767.

Vohradsky, J., Panek, J., and Vomastek, T. 2010. Numerical modelling of microRNA-mediated mRNA decay identifies novel mechanism of microRNA controlled mRNA downregulation. *Nucleic Acids Res.* 38, 4579-4585.

Vu, T.T., and Vohradsky, J. 2007. Nonlinear differential equation model for quantification of transcriptional regulation applied to microarray data of Saccharomyces cerevisiae. *Nucleic Acids Res.* 35, 279-287.

Wu, C.I., Shen, Y., and Tang, T. 2009. Evolution under canalization and the dual roles of microRNAs: a hypothesis. *Genome Res.* 19, 734-743.

Table 1. Summary of selected FFLs and their estimated parameters using Model M2.

Model M2												
	TF		miRNA		target mRNA	a_2 (CV)	a_3 (CV)	d_2 (CV)	p (CV)	q (CV)	r (CV)	C/I
1	hif1a	x	hsa-miR-24		h41	1.22 (74)	2.83 (44)	0.96 (79)	1.10 (67)	2.17 (52)	0.87 (78)	I
2	srf		hsa-miR-100		impdh1	1.40 (41)	0.68 (59)	0.57 (54)	0.91 (27)	0.34 (63)	0.84 (30)	I
3	tcf4		hsa-miR-23a		ndufa7	0.47 (62)	0.77 (44)	0.30 (83)	1.04 (21)	0.66 (42)	1.29 (69)	I
mean (absolute values)						1.03 (59)	1.43 (49)	0.61 (72)	1.02 (38)	1.06 (52)	0.85 (54)	
SE (absolute values)						0.49 (17)	1.22 (9)	0.33 (16)	0.10 (25)	0.98 (11)	0.25 (26)	

TF, miRNA and target mRNA names of selected FFLs using model M2 are reported along with the estimated parameters, their precision in terms of CV and a flag to distinguish between coherent (C) and incoherent (I) FFLs. TF and miRNA already known to be key regulators of adipogenesis and adipocyte-related functions are marked with an x.

Table 2. Summary of selected FFLs and their estimated parameters using Model M3.

Model M3											
	TF		miRNA		target mRNA	a_2 (CV)	a_3 (CV)	d_2 (CV)	d_3 (CV)	s (CV)	C/I
1	runx1		hsa-miR-148b		tnfrsf6b	-0.07 (17)	-1.73 (50)	-	8.28 (25)	4.49 (43)	I
2	runx1		hsa-miR-148b		loc51026	-0.07 (17)	2.70 (9)	-	2.85 (1)	2.70 (76)	C
3	runx1		hsa-miR-148b		tmod	-0.07 (17)	-1.79 (37)	-	3.70 (13)	1.44 (76)	I
4	esr1	x	hsa-miR-148b		map1b	0.14 (18)	1.69 (60)	-	2.49 (6)	4.49 (29)	I
5	esr1	x	hsa-miR-148b		tparl	0.15 (18)	-2.00 (48)	-	2.89 (2)	2.78 (42)	C
6	esr1	x	hsa-miR-148b		apt6m8-9	0.15 (18)	5.37 (33)	-	2.04 (19)	2.41 (41)	I
7	esr1	x	hsa-miR-152		apt6m8-9	0.42 (39)	3.94 (19)	0.16 (67)	1.12 (7)	1.55 (35)	I
8	esr1	x	hsa-miR-30c	x	emp1	0.65 (21)	-4.58 (28)	0.09 (46)	2.16 (5)	1.76 (40)	C
9	ets1		hsa-miR-199a*		hke2	-0.22 (17)	-1.60 (80)	0.90 (17)	0.35 (99)	7.52 (73)	I
10	hif1a	x	hsa-miR-199b		crtl1	-2.32 (59)	-4.99 (24)	1.26 (63)	0.97 (96)	2.47 (27)	I
11	hif1a	x	hsa-miR-24		h41	1.21 (34)	6.02 (35)	0.93 (35)	1.87 (16)	4.21 (46)	I
12	hif1a	x	hsa-miR-199a	x	crtl1	-2.17 (30)	-3.05 (45)	1.19 (25)	1.27 (19)	1.25 (63)	I
13	foxm1		hsa-let-7a		nap1l1	-0.02 (3)	-0.89 (29)	0.14 (58)	1.70 (3)	14.10 (52)	I
14	irf1		hsa-miR-29a	x	timm8b	-0.40 (7)	-5.00 (34)	-	2.23 (34)	0.60 (37)	I
15	irf7		hsa-miR-129		hs6st	-0.04 (82)	2.53 (37)	-	2.38 (6)	13.93 (89)	C
16	irf2		hsa-miR-125b		bcl2	-0.33 (16)	6.07 (23)	-	3.27 (3)	1.55 (45)	C
17	myc	x	hsa-miR-202		tnfrsf4	0.08 (42)	0.34 (92)	-	1.20 (95)	4.44 (87)	I
18	myod1		hsa-miR-34a	x	kcnq1	-0.30 (22)	-2.03 (27)	0.14 (35)	1.49 (24)	2.04 (29)	I
19	myod1		hsa-miR-34a	x	scn2b	-0.28 (21)	-2.00 (27)	0.12 (37)	4.61 (5)	0.58 (88)	I
20	ncx		hsa-let-7e	x	nap1l1	0.13 (67)	8.38 (14)	0.08 (87)	3.17 (3)	10.61 (76)	I
21	nfya		hsa-miR-148b		p3	-0.17 (18)	-1.66 (88)	-	4.05 (6)	4.73 (29)	I
22	tcf4		hsa-miR-23a		ndufa7	0.50 (66)	0.84 (54)	0.33 (89)	1.05 (28)	0.60 (75)	I
23	tel2		hsa-miR-199a*		hke2	0.65 (37)	6.91 (22)	0.34 (41)	1.34 (5)	4.41 (30)	I
mean (absolute values)						0.46 (30)	3.31 (40)	0.47 (50)	2.46 (23)	4.12 (53)	
SE (absolute values)						0.63 (21)	2.19 (22)	0.46 (23)	1.66 (31)	3.91 (22)	

TF, miRNA and target mRNA names of selected FFLs using model M3 are reported along with the estimated parameters, their precision in terms of CV and a flag to distinguish between coherent (C) and incoherent (I) FFLs. TF and miRNA already known to be key regulators of adipogenesis and adipocyte-related functions are marked with an x. When the estimated degradation parameter (d_2) was small and with low precision, i.e. the process was too slow to be determined in the time horizon of the experiment, it was set to 0 and model identification was repeated.

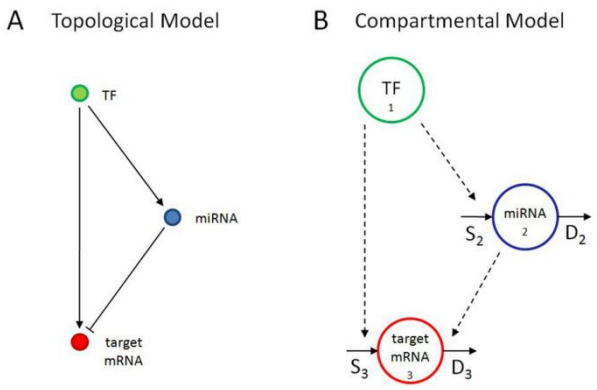

FIG. 1 MiRNA mediated FFL. (A) Topologial model of the FFL where a TF regulates a miRNA and they both regulate the target mRNA: TF regulations can be positive or negative while miRNA regulation of the target gene is negative; (B) compartmental model of the FFL where S and D represents synthesis and degradation, respectively and dotted arrows are the regulation processes affecting S and D.

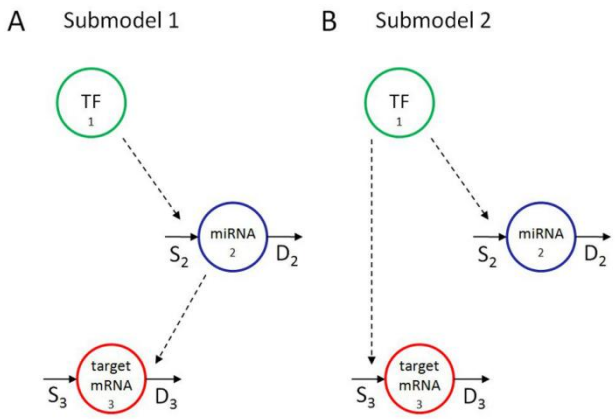

FIG. 2 Submodels with missing regulatory links with respect to the FFL. (A) No effect of TF regulation on target gene; (B) no effect of miRNA on mRNA degradation rate.

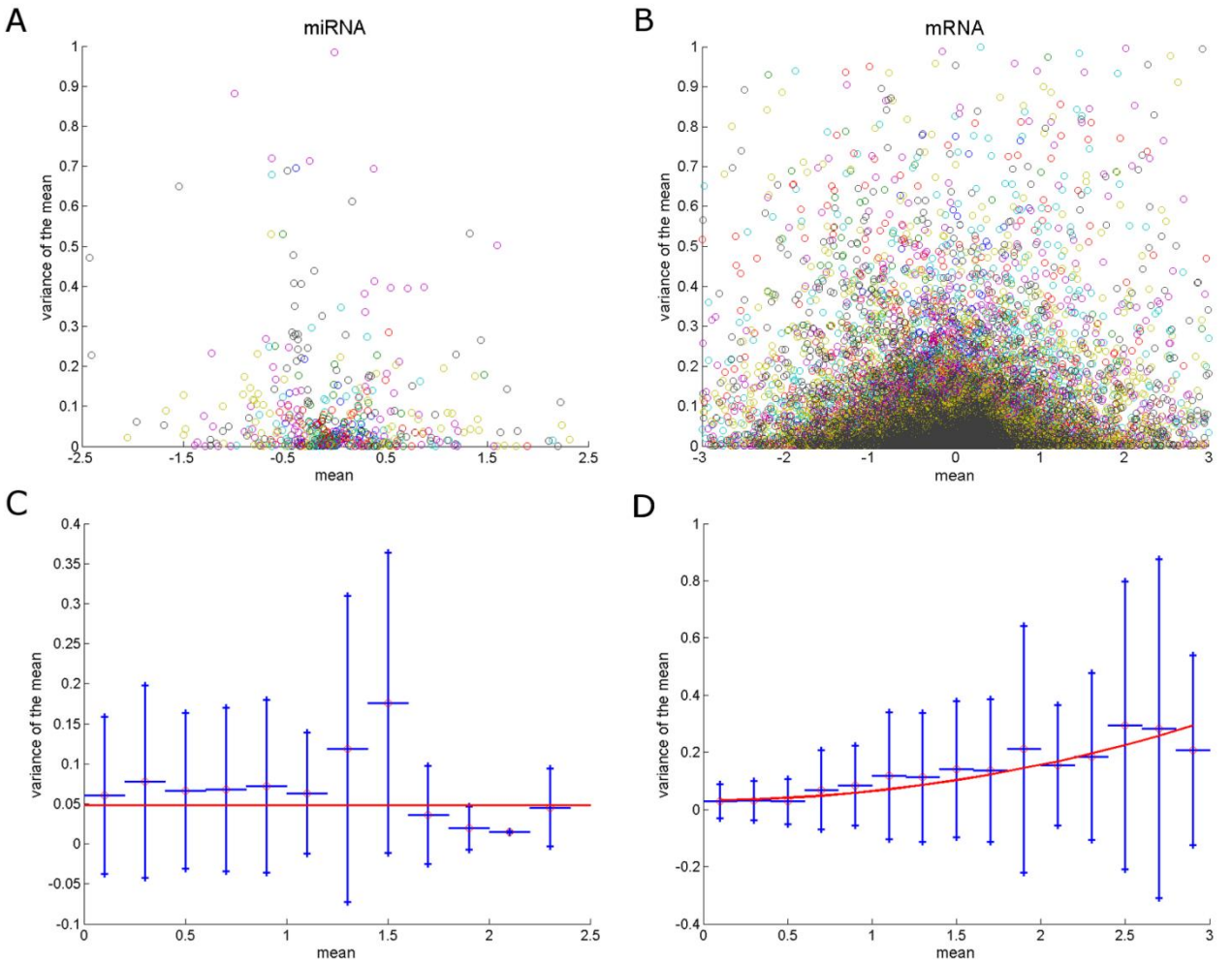

FIG. 3 Measurement error variance against expression estimated from the replicates for (A) miRNA and (B) mRNA datasets. In (C) and (D) these data are binned and, for each interval, the mean ± standard deviation is represented; the red line shows the fitted measurement error models, Equations 10.

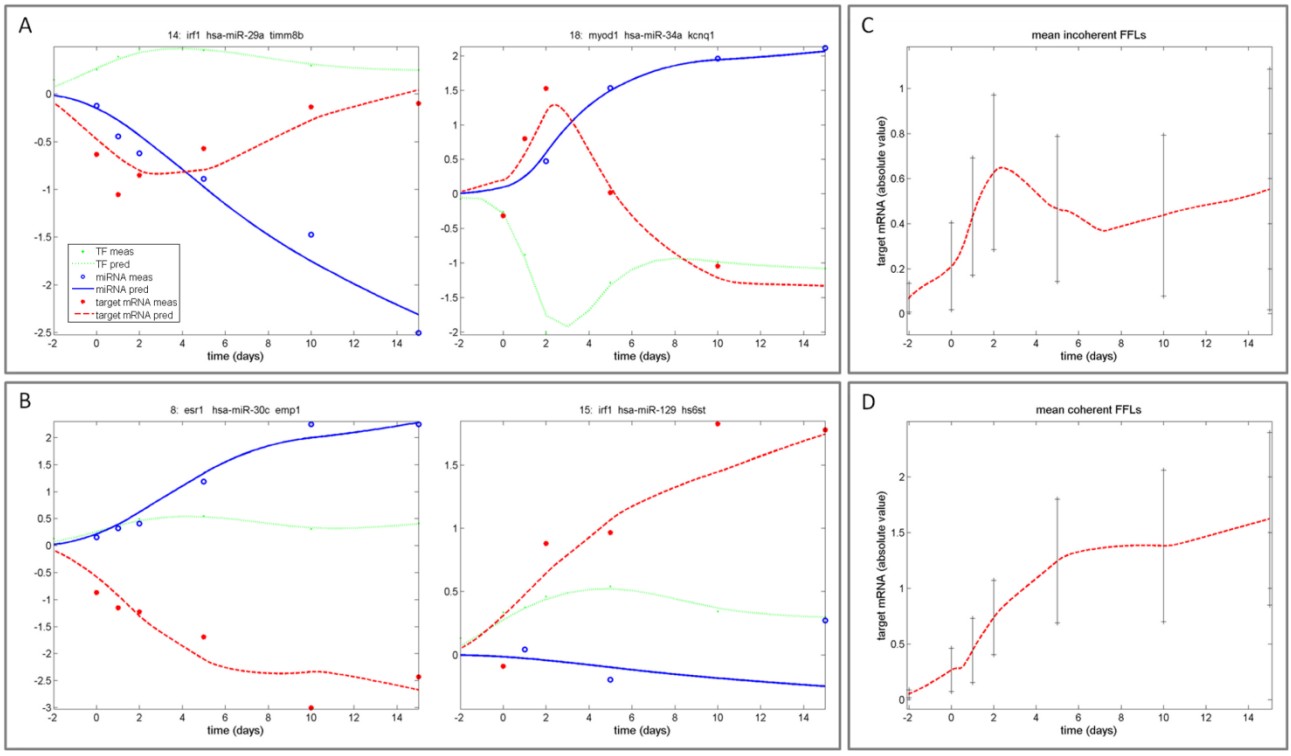

FIG. 4 Expression profiles of selected FFLs. TF (green), miRNA (blue) and target mRNA (red) for (A) 2 incoherent and (B) 2 coherent FFLs: spots represent experimental data while lines represent the predicted/reconstructed profiles. In (C) and (D) the average absolute value of predicted target mRNA expression for incoherent and coherent FFLs.

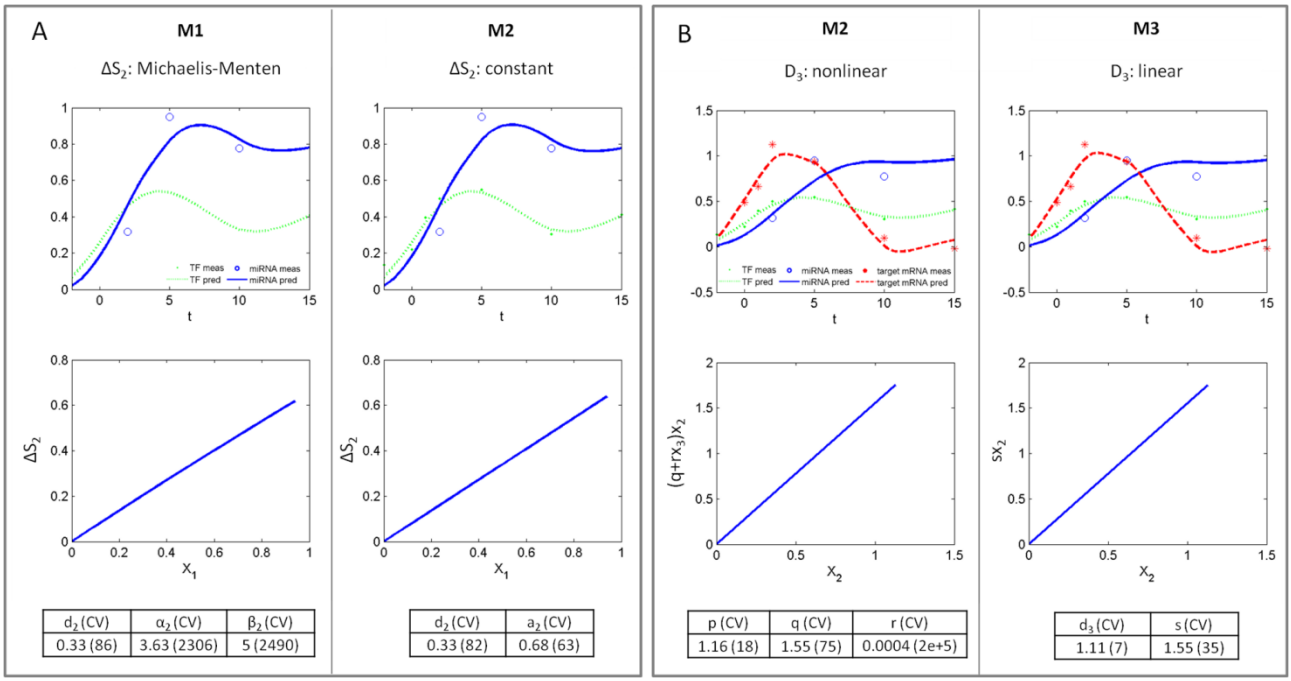

FIG. 5. Comparison between the candidate models. (A) upper panels: similarity between models M1 and M2 predictions for miRNA (blue) profile indicates that the Michaelis-Menten function is not necessary; lower panels: confirmation that the model prediction of the link between TF and miRNA, postulated as linear for M2, is operating in the linear range for M1; (B) upper panels: similarity between M2 and M3 predictions for target mRNA (red) profile suggests that a linear description of target mRNA degradation is sufficient; lower panel: confirmation that the miRNA mediated degradation rate, postulated as linear for M3, is operating in the linear range for M2.

Supplementary Material

Differential equations

Passages for the derivation of differential equations of Models M1, M2 and M3 (Equations (3), (4) and (5)) from the general functional description of Equation (2) are described in the follow. The three models adopt the same description for $\mathrm{D_2[X_2(t)] = d_2X_2(t)}$ while they adopt different functional descriptions for $\Delta \mathrm{S_i}$ i=2,3 and $\mathrm{D_3}$.

Model M1

$$\Delta S_i[X_1(t)] = \frac{\alpha'_i X_1(t)}{\beta'_i + X_1(t)} \qquad i = 2,3$$

$$D_3[X_2(t), X_3(t)] = \big(p' + rX_2(t)\big)X_3(t)$$

Thus, the system of differential equations is

$$\dot{X}_2(t) = S_{2b} + \frac{\alpha'_2 X_1(t)}{\beta'_2 + X_1(t)} - d_2 X_2(t) \qquad X_2(0) = X_{2b}$$

$$\dot{X}_3(t) = S_{3b} + \frac{\alpha'_3 X_1(t)}{\beta'_3 + X_1(t)} - \big(p' + rX_2(t)\big)X_3(t) \qquad X_3(0) = X_{3b}$$

Considering that at the basal state $\dot{X}_i(t) = 0$ for i=2,3 it is possible to express the basal transcriptions S_i as:

$$S_{2b} = -\frac{\alpha'_2 X_{1b}}{\beta'_2 + X_{1b}} + d_2 X_{2b}$$

$$S_{3b} = -\frac{\alpha'_3 X_{1b}}{\beta'_3 + X_{1b}} + (p' + rX_{2b})X_{3b}$$

and substituting S_i in the differential equations we obtain:

$$\dot{X}_2(t) = \frac{\alpha_2' X_1(t)}{\beta_2' + X_1(t)} - \frac{\alpha_2' X_{1b}}{\beta_2' + X_{1b}} - d_2 X_2(t) + d_2 X_{2b}$$

$$= \frac{\alpha_2' \beta_2' (X_1(t) - X_{1b})}{(\beta_2' + X_1(t))(\beta_2' + X_{1b})} - d_2 (X_2(t) - X_{2b})$$

$$\dot{X}_3(t) = \frac{\alpha_3' X_1(t)}{\beta_3' + X_1(t)} - \frac{\alpha_3' X_{1b}}{\beta_3' + X_{1b}} - \big(p' + rX_2(t)\big)X_3(t) + (p' + rX_{2b})X_{3b} =$$

$$= \frac{\alpha_3' \beta_3' (X_1(t) - X_{1b})}{(\beta_3' + X_1(t))(\beta_3' + X_{1b})} - p'(X_3(t) - X_{3b}) - r(X_2(t)X_3(t) - X_{2b}X_{3b})$$

Considering as state variables $x_i = X_i - X_{ib}$ for i=1,2,3 differential equations turn out to be

$$\dot{x}_2(t) = \frac{\alpha_2 x_1(t)}{\beta_2 + x_1(t)} - d_2 x_2(t) \qquad x_2(0) = 0$$

$$\dot{x}_3(t) = \frac{\alpha_3 x_1(t)}{\beta_3 + x_1(t)} - p x_3(t) - q x_2(t) - r x_2(t) x_3(t) \qquad x_3(0) = 0$$

where for i=2,3 $\alpha_i = \frac{\alpha_i' \beta_i'}{\beta_i' + X_{1b}}$, $\beta_i = \beta_i' + X_{1b}$, $p = p' + rX_{2b}$, $q = rX_{3b}$.

Model M2

$\Delta S_i[X_1(t)] = a_i X_1(t) \qquad i = 2,3$

$D_3[X_2(t), X_3(t)] = \big(p' + rX_2(t)\big)X_3(t)$

Thus, the system of differential equations is

$$\dot{X}_2(t) = S_{2b} + a_2 X_1(t) - d_2 X_2(t) \qquad X_2(0) = X_{2b}$$

$$\dot{X}_3(t) = S_{3b} + a_3 X_1(t) - \big(p' + rX_2(t)\big)X_3(t) \qquad X_3(0) = X_{3b}$$

Considering that at the basal state $\dot{X}_i(t) = 0$ for i=2,3 it is possible to express the basal transcriptions S_i as:

$$S_{2b} = -a_2 X_{1b} + d_2 X_{2b}$$

$$S_{3b} = -a_3 X_{1b} + (p' + rX_{2b})X_{3b}$$

Substituting S_i and considering as state variables $x_i = X_i - X_{ib}$ for i=1,2,3 differential equations turn out to be:

$$\dot{x}_2(t) = a_2 x_1(t) - d_2 x_2(t) \qquad x_2(0) = 0$$

$$\dot{x}_3(t) = a_3 x_1(t) - p x_3(t) - q x_2(t) - r x_2(t) x_3(t) \qquad x_3(0) = 0$$

where $p = p' + rX_{2b}$, $q = rX_{3b}$ are the same reparametrizations used in Model M1.

Model M3

$\Delta S_i[X_1(t)] = a_i X_1(t) \qquad i = 2,3$

$D_3[X_2(t), X_3(t)] = d_3 X_3(t) + sX_2(t)$

Thus, the system of differential equations is

$$\dot{X}_2(t) = S_{2b} + a_2 X_1(t) - d_2 X_2(t) \qquad X_2(0) = X_{2b}$$

$$\dot{X}_3(t) = S_{3b} + a_3 X_1(t) - d_3 X_3(t) - sX_2(t) \qquad X_3(0) = X_{3b}$$

Considering that at the basal state $\dot{X}_i(t) = 0$ for i=2,3 it is possible to express the basal transcriptions S_i as:

$$S_{2b} = -a_2 X_{1b} + d_2 X_{2b}$$

$$S_{3b} = -a_3 X_{1b} + d_3 X_{3b} + sX_{2b}$$

Substituting S_i and considering as state variables $x_i = X_i - X_{ib}$ for i=1,2,3 differential equations turn out to be:

$$\dot{x}_2(t) = a_2 x_1(t) - d_2 x_2(t) \qquad x_2(0) = 0$$

$$\dot{x}_3(t) = a_3 x_1(t) - d_3 x_3(t) - s x_2(t) \qquad x_3(0) = 0$$

Implementation details

Parameters of both FFLs and measurement error models, as well as their precision, are estimated using the standard trust-region-reflective algorithm implemented by the lsqnonlin function of Matlab to solve the least square problem, while differential equations are solved numerically using Runge-Kutta (4,5) procedure implemented by the ode45 function of Matlab. The TF expression profile is used as forcing function and a smoothing approach, taking into account the measurement error, is applied to numerically approximate its time continuous dynamic. The Weighted Least Square optimization procedure is repeated for different initial conditions and the set of parameters which gave the best prediction of miRNA and target mRNA expression time series is selected to minimize the possibility of incurring in a local minimum. All computations are performed in the Matlab environment (Matlab R2010a).

Selected FFLs

None of the identified feed forward loop is known in the literature and further biological validation, beyond the scope of this work, should be done to confirm these hypothesis. However, our FFLs selection contains a considerable number of genes with known adipogenesis- or adipocyte-related function, which supports the validity of the proposed method.

The transcription factor estrogen receptor 1, ESR1, (FFLs 4-9, Table 2) is a critical regulator in white adipose tissue (WAT), as its absence results in marked increases in WAT as well as in insulin resistance and impaired glucose tolerance (Heine, et al., 2000). Interestingly, we found miR-30c and ESR1 involved in the same FFL. In the context of estrogen receptor positive breast cancer, these two genes have been identified to be positively correlated (Rodriguez-Gonzalez, et al., 2010). Moreover, miR-30c has recently been shown to directly bind and repress plasminogen activator inhibitor 1 (PAI-1) (Patel, et al., 2010), an adipose derived cytokine (Morange, et al., 1999) and predictor for the risk of developing type 2 diabetes (Festa, et al., 2002) elevated in

serum of obese humans (Estelles, et al., 2001). The transcription factor hypoxia-inducible factor 1 alpha, HIF1A, (FFLs 10-12, Table 2), inhibits the adipogenic key regulator peroxisome proliferator-activated receptor gamma 2 (PPARG2) (Yun, et al., 2002). Moreover, hypoxia-induced insulin resistance in adipocytes is dependent upon HIF1A expression (Regazzetti, et al., 2009). miR-29a (FFL 14, Table 2) has been found to be highly up-regulated in adipose tissue of diabetic rats, and positively correlated to insulin resistance and impaired insulin-stimulated glucose uptake in 3T3 L1 adipocytes (He, et al., 2007). The transcription factor and oncogene MYC (FFL 17, Table 2) has been previously found to inhibit the expression of genes that promote adipogenesis, in particular of CCAAT/enhancer-binding protein alpha (CEBPA), a transcription factor that promotes adipogenesis (Freytag and Geddes, 1992). miR-34a (FFLs 18-19, Table 2) is associated with obesity as it has been shown to target hepatic SIRT1 and to suppress insulin secretion in pancreatic β-cells (Lee, et al., 2010; Lovis, et al., 2008). let-7a (FFL 20, Table 2) regulates the transition from clonal expansion to terminal differentiation (Sun, et al., 2009).

Finally, miR-24 (FFL 1, Table 1), although not yet associated to adipogenesis, is known to be induced by hypoxia and HIF1A (Kulshreshtha, et al., 2007) and is located in a cluster together with miR-27b which we already have identified as repressor of the adipogenic key regulator PPARγ in human (Karbiener, et al., 2009).

Putative FFLs

Table 1. Putative FFLs

	TF	miRNA	target gene	
1	AML1	hsa-miR-202	ENSG00000056345	ITGB3
2	AML1	hsa-miR-202	ENSG00000164654	NP_061878.3
3	AML1	hsa-miR-202	ENSG00000186827	TNFRSF4
4	AML1	hsa-miR-148b	ENSG00000026036	TNFRSF6B
5	AML1	hsa-miR-148b	ENSG00000111711	GOLT1B
6	AML1	hsa-miR-148b	ENSG00000130052	STARD8

7	AML1	hsa-miR-148b	ENSG00000135374	ELF5
8	AML1	hsa-miR-148b	ENSG00000136842	TMOD1
9	AML1	hsa-miR-148b	ENSG00000137073	UBAP2
10	AML1	hsa-miR-31	ENSG00000013588	GPRC5A
11	AML1	hsa-miR-31	ENSG00000073969	NSF
12	AML1	hsa-miR-31	ENSG00000100612	DHRS7
13	AML1	hsa-miR-10a	ENSG00000147082	CCNB3
14	AP-1	hsa-miR-199a	ENSG00000170430	MGMT
15	ATF-1	hsa-miR-199b	ENSG00000108515	ENO3
16	ATF-1	hsa-miR-199a*	ENSG00000100109	TFIP11
17	ATF-1	hsa-miR-199a	ENSG00000108515	ENO3
18	ATF6	hsa-miR-214	ENSG00000167468	GPX4
19	DBP	hsa-miR-29a	ENSG00000185650	ZFP36L1
20	EGR	hsa-miR-193a	ENSG00000012779	ALOX5
21	EGR	hsa-miR-193a	ENSG00000084090	STARD7
22	EGR	hsa-miR-193a	ENSG00000137478	FCHSD2
23	ER	hsa-miR-148b	ENSG00000034063	UHRF1
24	ER	hsa-miR-148b	ENSG00000070985	TRPM5
25	ER	hsa-miR-148b	ENSG00000105366	SIGLEC8
26	ER	hsa-miR-148b	ENSG00000113048	MRPS27
27	ER	hsa-miR-148b	ENSG00000131711	MAP1B
28	ER	hsa-miR-148b	ENSG00000134851	TMEM165
29	ER	hsa-miR-148b	ENSG00000137073	UBAP2
30	ER	hsa-miR-148b	ENSG00000156642	NPTN
31	ER	hsa-miR-148b	ENSG00000156642	NPTN
32	ER	hsa-miR-148b	ENSG00000182220	ATP6AP2
33	ER	hsa-miR-129	ENSG00000105058	FAM32A
34	ER	hsa-miR-129	ENSG00000119772	DNMT3A
35	ER	hsa-miR-129	ENSG00000136720	HS6ST1
36	ER	hsa-miR-129	ENSG00000145416	MARCH1
37	ER	hsa-miR-152	ENSG00000034063	UHRF1
38	ER	hsa-miR-152	ENSG00000070985	TRPM5
39	ER	hsa-miR-152	ENSG00000105366	SIGLEC8
40	ER	hsa-miR-152	ENSG00000113048	MRPS27
41	ER	hsa-miR-152	ENSG00000131711	MAP1B
42	ER	hsa-miR-152	ENSG00000134851	TMEM165
43	ER	hsa-miR-152	ENSG00000137073	UBAP2
44	ER	hsa-miR-152	ENSG00000156642	NPTN
45	ER	hsa-miR-152	ENSG00000156642	NPTN
46	ER	hsa-miR-152	ENSG00000182220	ATP6AP2
47	ER	hsa-miR-30c	ENSG00000033867	SLC4A7
48	ER	hsa-miR-30c	ENSG00000079739	PGM1

49	ER	hsa-miR-30c	ENSG00000134531	EMP1
50	ER	hsa-miR-30c	ENSG00000138069	RAB1A
51	ER	hsa-miR-130a	ENSG00000070985	TRPM5
52	ER	hsa-miR-130a	ENSG00000077312	SNRPA
53	ER	hsa-miR-130a	ENSG00000086015	MAST2
54	ER	hsa-miR-130a	ENSG00000103723	AP3B2
55	ER	hsa-miR-130a	ENSG00000113048	MRPS27
56	ER	hsa-miR-130a	ENSG00000120509	PDZD11
57	ER	hsa-miR-130a	ENSG00000123395	C12orf44
58	ER	hsa-miR-130a	ENSG00000137073	UBAP2
59	ER	hsa-miR-130a	ENSG00000138641	HERC3
60	ER	hsa-miR-130a	ENSG00000147642	SYBU_HUMAN
61	ER	hsa-miR-130a	ENSG00000156642	NPTN
62	ER	hsa-miR-130a	ENSG00000156642	NPTN
63	ER	hsa-miR-130a	ENSG00000157077	ZFYVE9
64	ER	hsa-miR-130a	ENSG00000182220	ATP6AP2
65	ETS	hsa-miR-199a*	ENSG00000116141	MARK1
66	ETS	hsa-miR-199a*	ENSG00000204220	PFDN6
67	ETS	hsa-miR-24	ENSG00000114019	AMOTL2
68	GABP	hsa-miR-148b	ENSG00000111711	GOLT1B
69	GABP	hsa-miR-148b	ENSG00000115310	RTN4
70	GABP	hsa-miR-148b	ENSG00000131711	MAP1B
71	GABP	hsa-miR-148b	ENSG00000136842	TMOD1
72	GABP	hsa-miR-148b	ENSG00000151694	ADAM17
73	GABP	hsa-miR-130a	ENSG00000111711	GOLT1B
74	GABP	hsa-miR-130a	ENSG00000115310	RTN4
75	GABP	hsa-miR-130a	ENSG00000152291	TGOLN2
76	GABP	hsa-miR-130a	ENSG00000164896	FASTK
77	HIF-1	hsa-miR-199b	ENSG00000108515	ENO3
78	HIF-1	hsa-miR-199b	ENSG00000145681	HAPLN1
79	HIF-1	hsa-miR-199b	ENSG00000176986	SEC24C
80	HIF-1	hsa-miR-24	ENSG00000091527	CDV3
81	HIF-1	hsa-miR-24	ENSG00000124702	KLHDC3
82	HIF-1	hsa-miR-24	ENSG00000135924	DNAJB2
83	HIF-1	hsa-miR-24	ENSG00000142188	TMEM50B
84	HIF-1	hsa-miR-214	ENSG00000116649	SRM
85	HIF-1	hsa-miR-214	ENSG00000167468	GPX4
86	HIF-1	hsa-miR-214	ENSG00000171551	ECEL1
87	HIF-1	hsa-miR-199a	ENSG00000108515	ENO3
88	HIF-1	hsa-miR-199a*	ENSG00000136928	GABBR2
89	HIF-1	hsa-miR-199a	ENSG00000145681	HAPLN1
90	HIF-1	hsa-miR-199a	ENSG00000176986	SEC24C

91	HNF-1	hsa-miR-494	ENSG00000149575	SCN2B
92	HNF-1	hsa-miR-494	ENSG00000149575	SCN2B
93	HNF-1	hsa-miR-381	ENSG00000102158	IAG2_HUMAN
94	HNF-1	hsa-miR-381	ENSG00000116833	NR5A2
95	HNF-1	hsa-miR-381	ENSG00000141720	PIP5K2B
96	HNF-1	hsa-miR-381	ENSG00000145495	MARCH6
97	HNF-1	hsa-miR-381	ENSG00000204304	PBX2
98	HNF-1	hsa-miR-299-5p	ENSG00000049130	KITLG
99	HNF-1	hsa-miR-299-5p	ENSG00000049130	KITLG
100	HNF-1	hsa-miR-299-5p	ENSG00000067798	NAV3
101	HNF-1	hsa-miR-299-5p	ENSG00000140263	SORD
102	HNF-1	hsa-miR-487b	ENSG00000104341	LAPTM4B
103	HNF-1	hsa-miR-487b	ENSG00000104341	LAPTM4B
104	HNF-3	hsa-let-7f	ENSG00000118971	CCND2
105	HNF-3	hsa-let-7f	ENSG00000164654	NP_061878.3
106	HNF-3	hsa-let-7f	ENSG00000172053	QARS
107	HNF-3	hsa-let-7f	ENSG00000187109	NAP1L1
108	HNF-3	hsa-miR-129	ENSG00000120533	ENY2
109	HNF-3	hsa-miR-129	ENSG00000145416	MARCH1
110	HNF-3	hsa-let-7d	ENSG00000149313	AASDHPPT
111	HNF-3	hsa-let-7d	ENSG00000172053	QARS
112	HNF-3	hsa-let-7a	ENSG00000118971	CCND2
113	HNF-3	hsa-let-7a	ENSG00000164654	NP_061878.3
114	HNF-3	hsa-let-7a	ENSG00000172053	QARS
115	HNF-3	hsa-let-7a	ENSG00000187109	NAP1L1
116	HNF-3	hsa-miR-31	ENSG00000156711	MAPK13
117	HOXA4	hsa-miR-129	ENSG00000105058	FAM32A
118	HOXA4	hsa-miR-148b	ENSG00000182220	ATP6AP2
119	HOXA4	hsa-miR-125b	ENSG00000065361	ERBB3
120	HOXA4	hsa-miR-125b	ENSG00000106993	CDC37L1
121	HOXA4	hsa-miR-125b	ENSG00000110274	CEP164
122	HOXA4	hsa-miR-125b	ENSG00000172531	PPP1CA
123	HOXA4	hsa-miR-296	ENSG00000138823	MTTP
124	IRF1	hsa-miR-29a	ENSG00000147065	MSN
125	IRF1	hsa-miR-29a	ENSG00000150779	TIMM8B
126	IRF-7	hsa-miR-129	ENSG00000136720	HS6ST1
127	IRF-7	hsa-miR-129	ENSG00000158435	C2orf29
128	IRF-7	hsa-miR-129	ENSG00000170310	STX8
129	IRF	hsa-let-7d	ENSG00000110583	NAT11
130	IRF	hsa-let-7d	ENSG00000110583	NAT11
131	IRF	hsa-let-7d	ENSG00000110583	NAT11
132	IRF	hsa-let-7d	ENSG00000110583	NAT11

133	IRF	hsa-miR-125b	ENSG00000171791	BCL2
134	IRF	hsa-miR-125b	ENSG00000171791	BCL2
135	IRF	hsa-miR-125b	ENSG00000171791	BCL2
136	IRF	hsa-miR-125b	ENSG00000171791	BCL2
137	IRF	hsa-miR-100	ENSG00000118689	FOXO3A
138	IRF	hsa-miR-100	ENSG00000118689	FOXO3A
139	IRF	hsa-miR-100	ENSG00000118689	FOXO3A
140	IRF	hsa-miR-100	ENSG00000118689	FOXO3A
141	IRF	hsa-miR-100	ENSG00000162437	RAVER2
142	IRF	hsa-miR-100	ENSG00000162437	RAVER2
143	IRF	hsa-miR-100	ENSG00000162437	RAVER2
144	IRF	hsa-miR-100	ENSG00000162437	RAVER2
145	MAZ	hsa-let-7a	ENSG00000023902	PLEKHO1
146	MAZ	hsa-let-7a	ENSG00000106367	AP1S1
147	MAZ	hsa-miR-34a	ENSG00000142319	SLC6A3
148	MAZ	hsa-let-7b	ENSG00000023902	PLEKHO1
149	MAZ	hsa-let-7b	ENSG00000106367	AP1S1
150	MEIS1	hsa-let-7e	ENSG00000023902	PLEKHO1
151	MEIS1	hsa-let-7e	ENSG00000085491	SLC25A24
152	MEIS1	hsa-let-7e	ENSG00000105697	HAMP
153	MEIS1	hsa-let-7e	ENSG00000118503	TNFAIP3
154	MEIS1	hsa-let-7e	ENSG00000119906	C10orf6
155	MEIS1	hsa-let-7e	ENSG00000143851	PTPN7
156	MEIS1	hsa-let-7e	ENSG00000187109	NAP1L1
157	MEIS1	hsa-let-7a	ENSG00000023902	PLEKHO1
158	MEIS1	hsa-let-7a	ENSG00000119906	C10orf6
159	MEIS1	hsa-let-7a	ENSG00000143851	PTPN7
160	MEIS1	hsa-let-7a	ENSG00000187109	NAP1L1
161	MEIS1	hsa-let-7a	ENSG00000023902	PLEKHO1
162	MEIS1	hsa-let-7a	ENSG00000119906	C10orf6
163	MEIS1	hsa-let-7a	ENSG00000143851	PTPN7
164	MEIS1	hsa-let-7a	ENSG00000187109	NAP1L1
165	MEIS1	hsa-miR-30c	ENSG00000079739	PGM1
166	MEIS1	hsa-miR-30c	ENSG00000145725	HISPPD1
167	MEIS1	hsa-miR-30c	ENSG00000154274	C4orf19
168	MEIS1	hsa-miR-30c	ENSG00000170365	SMAD1
169	MEIS1	hsa-miR-99b	ENSG00000116017	ARID3A
170	MEIS1	hsa-miR-99b	ENSG00000162437	RAVER2
171	MEIS1	hsa-miR-30a-5p	ENSG00000079739	PGM1
172	MEIS1	hsa-miR-30a-5p	ENSG00000145725	HISPPD1
173	MEIS1	hsa-miR-30a-5p	ENSG00000154274	C4orf19
174	MEIS1	hsa-miR-30a-5p	ENSG00000170365	SMAD1

175	MEIS1	hsa-miR-125b	ENSG00000087916	SLC6A14
176	MEIS1	hsa-miR-125b	ENSG00000110274	CEP164
177	MEIS1	hsa-miR-125b	ENSG00000120656	TAF12
178	MEIS1	hsa-miR-125b	ENSG00000123064	DDX54
179	MEIS1	hsa-miR-125b	ENSG00000133561	GIMAP6
180	MEIS1	hsa-miR-125b	ENSG00000196616	ADH1C
181	MEIS1	hsa-let-7b	ENSG00000023902	PLEKHO1
182	MEIS1	hsa-let-7b	ENSG00000119906	C10orf6
183	MEIS1	hsa-let-7b	ENSG00000143851	PTPN7
184	MEIS1	hsa-let-7b	ENSG00000187109	NAP1L1
185	MEIS1	hsa-miR-214	ENSG00000058668	ATP2B4
186	MEIS1	hsa-miR-214	ENSG00000082556	OPRK1
187	MEIS1	hsa-miR-214	ENSG00000110851	PRDM4
188	MEIS1	hsa-miR-214	ENSG00000147892	ADAMTSL1
189	MEIS1	hsa-miR-214	ENSG00000167468	GPX4
190	MEIS1	hsa-miR-214	ENSG00000171303	KCNK3
191	MEIS1	hsa-miR-214	ENSG00000173020	ADRBK1
192	MEIS1	hsa-miR-296	ENSG00000090097	PCBP4
193	MEIS1	hsa-miR-296	ENSG00000101246	ARFRP1
194	MEIS1	hsa-miR-296	ENSG00000167680	SEMA6B
195	MEIS1	hsa-miR-125b	ENSG00000087916	SLC6A14
196	MEIS1	hsa-miR-125b	ENSG00000110274	CEP164
197	MEIS1	hsa-miR-125b	ENSG00000120656	TAF12
198	MEIS1	hsa-miR-125b	ENSG00000123064	DDX54
199	MEIS1	hsa-miR-125b	ENSG00000133561	GIMAP6
200	MEIS1	hsa-miR-125b	ENSG00000196616	ADH1C
201	MEIS1	hsa-miR-100	ENSG00000116017	ARID3A
202	MEIS1	hsa-miR-100	ENSG00000162437	RAVER2
203	MEIS1	hsa-miR-199a*	ENSG00000005884	ITGA3
204	MEIS1	hsa-miR-199a*	ENSG00000072401	UBE2D1
205	MEIS1	hsa-miR-199a*	ENSG00000085511	MAP3K4
206	MEIS1	hsa-miR-199a*	ENSG00000104067	TJP1
207	MEIS1	hsa-miR-199a*	ENSG00000105329	TGFB1
208	MEIS1	hsa-miR-199a	ENSG00000129116	PALLD
209	MEIS1	hsa-miR-199a*	ENSG00000132963	POMP
210	MEIS1	hsa-miR-199a*	ENSG00000140598	EFTUD1
211	MEIS1	hsa-miR-199a*	ENSG00000146021	KLHL3
212	MEIS1	hsa-miR-199a*	ENSG00000165156	ZHX1
213	MEIS1	hsa-miR-199a	ENSG00000170430	MGMT
214	MYC	hsa-miR-202	ENSG00000104660	LEPROTL1
215	MYC	hsa-miR-202	ENSG00000110583	NAT11
216	MYC	hsa-miR-202	ENSG00000119048	UBE2B

217	MYC	hsa-miR-202	ENSG00000143727	ACP1
218	MYC	hsa-miR-202	ENSG00000186827	TNFRSF4
219	MYC	hsa-miR-193a	ENSG00000054392	HHAT
220	MYC	hsa-miR-193a	ENSG00000078070	MCCC1
221	MYC	hsa-miR-193a	ENSG00000137478	FCHSD2
222	MYC	hsa-miR-193a	ENSG00000139641	FAM62A
223	MYC	hsa-miR-193a	ENSG00000185875	THNSL1
224	MYC	hsa-miR-193a	ENSG00000196084	UBIQ_HUMAN
225	MYC	hsa-miR-296	ENSG00000123933	MXD4
226	MYC	hsa-miR-296	ENSG00000167680	SEMA6B
227	MYOD	hsa-miR-542-3p	ENSG00000126214	KLC1
228	MYOD	hsa-miR-34a	ENSG00000053918	KCNQ1
229	MYOD	hsa-miR-34a	ENSG00000149575	SCN2B
230	MYOD	hsa-miR-34a	ENSG00000175592	FOSL1
231	MYOD	hsa-miR-34a	ENSG00000204619	PPP1R11
232	NCX	hsa-let-7e	ENSG00000125741	OPA3
233	NCX	hsa-let-7e	ENSG00000187109	NAP1L1
234	NCX	hsa-miR-99b	ENSG00000112299	VNN1
235	NCX	hsa-miR-542-3p	ENSG00000113580	NR3C1
236	NCX	hsa-miR-542-3p	ENSG00000142208	AKT1
237	NCX	hsa-miR-125b	ENSG00000089639	GMIP
238	NCX	hsa-miR-125b	ENSG00000106993	CDC37L1
239	NCX	hsa-miR-125b	ENSG00000153885	KCTD15
240	NF-Y	hsa-miR-148b	ENSG00000015592	STMN4
241	NF-Y	hsa-miR-148b	ENSG00000015592	STMN4
242	NF-Y	hsa-miR-148b	ENSG00000015592	STMN4
243	NF-Y	hsa-miR-148b	ENSG00000085433	WDR47
244	NF-Y	hsa-miR-148b	ENSG00000085433	WDR47
245	NF-Y	hsa-miR-148b	ENSG00000085433	WDR47
246	NF-Y	hsa-miR-148b	ENSG00000126903	SLC10A3
247	NF-Y	hsa-miR-148b	ENSG00000126903	SLC10A3
248	NF-Y	hsa-miR-148b	ENSG00000126903	SLC10A3
249	NF-Y	hsa-miR-148b	ENSG00000134851	TMEM165
250	NF-Y	hsa-miR-148b	ENSG00000134851	TMEM165
251	NF-Y	hsa-miR-148b	ENSG00000134851	TMEM165
252	NF-Y	hsa-miR-148b	ENSG00000172053	QARS
253	NF-Y	hsa-miR-148b	ENSG00000172053	QARS
254	NF-Y	hsa-miR-148b	ENSG00000172053	QARS
255	NF-Y	hsa-miR-148b	ENSG00000174851	YIF1A
256	NF-Y	hsa-miR-148b	ENSG00000174851	YIF1A
257	NF-Y	hsa-miR-148b	ENSG00000174851	YIF1A
258	NF-Y	hsa-miR-148b	ENSG00000182512	GLRX5

259	NF-Y	hsa-miR-148b	ENSG00000182512	GLRX5
260	NF-Y	hsa-miR-148b	ENSG00000182512	GLRX5
261	NF-Y	hsa-miR-148b	ENSG00000189266	PNRC2
262	NF-Y	hsa-miR-148b	ENSG00000189266	PNRC2
263	NF-Y	hsa-miR-148b	ENSG00000189266	PNRC2
264	NF-Y	hsa-miR-138	ENSG00000086712	CXorf15
265	NF-Y	hsa-miR-138	ENSG00000086712	CXorf15
266	NF-Y	hsa-miR-138	ENSG00000086712	CXorf15
267	NF-Y	hsa-miR-125b	ENSG00000110075	SAPS3
268	NF-Y	hsa-miR-125b	ENSG00000110075	SAPS3
269	NF-Y	hsa-miR-125b	ENSG00000110075	SAPS3
270	NF-Y	hsa-miR-125b	ENSG00000110274	CEP164
271	NF-Y	hsa-miR-125b	ENSG00000110274	CEP164
272	NF-Y	hsa-miR-125b	ENSG00000110274	CEP164
273	NF-Y	hsa-miR-125b	ENSG00000123064	DDX54
274	NF-Y	hsa-miR-125b	ENSG00000123064	DDX54
275	NF-Y	hsa-miR-125b	ENSG00000123064	DDX54
276	NF-Y	hsa-miR-125b	ENSG00000130348	QRSL1
277	NF-Y	hsa-miR-125b	ENSG00000130348	QRSL1
278	NF-Y	hsa-miR-125b	ENSG00000130348	QRSL1
279	NF-Y	hsa-miR-125b	ENSG00000138111	TMEM180
280	NF-Y	hsa-miR-125b	ENSG00000138111	TMEM180
281	NF-Y	hsa-miR-125b	ENSG00000138111	TMEM180
282	NF-Y	hsa-miR-125b	ENSG00000143390	RFX5
283	NF-Y	hsa-miR-125b	ENSG00000143390	RFX5
284	NF-Y	hsa-miR-125b	ENSG00000143390	RFX5
285	NF-Y	hsa-miR-125b	ENSG00000182858	ALG12
286	NF-Y	hsa-miR-125b	ENSG00000182858	ALG12
287	NF-Y	hsa-miR-125b	ENSG00000182858	ALG12
288	RORALPHA2	hsa-miR-125b	ENSG00000100599	RIN3
289	RORALPHA2	hsa-miR-125b	ENSG00000143390	RFX5
290	RREB-1	hsa-miR-148b	ENSG00000170989	EDG1
291	SREBP-1	hsa-miR-296	ENSG00000172354	GNB2
292	SRF	hsa-let-7a	ENSG00000135441	BLOC1S1
293	SRF	hsa-let-7a	ENSG00000135535	CD164
294	SRF	hsa-miR-214	ENSG00000171303	KCNK3
295	SRF	hsa-miR-125b	ENSG00000153885	KCTD15
296	SRF	hsa-miR-100	ENSG00000106348	IMPDH1
297	SRF	hsa-miR-100	ENSG00000138660	C4orf16
298	SRF	hsa-miR-100	ENSG00000153147	SMARCA5
299	SRF	hsa-miR-100	ENSG00000162437	RAVER2
300	SRF	hsa-miR-199a*	ENSG00000072401	UBE2D1

301	SRF	hsa-miR-199a*	ENSG00000132963	POMP
302	SRF	hsa-miR-199a*	ENSG00000182481	KPNA2
303	STAT1	hsa-miR-130a	ENSG00000152291	TGOLN2
304	STAT1	hsa-miR-130a	ENSG00000162998	FRZB
305	STAT1	hsa-miR-130a	ENSG00000164896	FASTK
306	STAT1	hsa-miR-130a	ENSG00000171703	TCEA2
307	STAT1	hsa-miR-130a	ENSG00000182512	GLRX5
308	STAT1	hsa-miR-130a	ENSG00000184371	CSF1
309	TCF-1(P)	hsa-miR-129	ENSG00000103326	SOLH
310	TCF-1(P)	hsa-miR-129	ENSG00000158435	C2orf29
311	TCF-1(P)	hsa-miR-129	ENSG00000169509	CRCT1
312	TCF-1(P)	hsa-miR-542-3p	ENSG00000071127	WDR1
313	TCF-1(P)	hsa-miR-542-3p	ENSG00000094916	CBX5
314	TCF-1(P)	hsa-miR-542-3p	ENSG00000145781	COMMD10
315	TCF-4	hsa-miR-10a	ENSG00000143198	MGST3
316	TCF-4	hsa-miR-10a	ENSG00000144681	STAC
317	TCF-4	hsa-miR-27a	ENSG00000130479	MAP1S
318	TCF-4	hsa-miR-23a	ENSG00000167774	NDUFA7
319	TEL-2	hsa-miR-199a*	ENSG00000204220	PFDN6
320	YY1	hsa-let-7a	ENSG00000071894	CPSF1
321	YY1	hsa-let-7a	ENSG00000187109	NAP1L1
322	YY1	hsa-miR-16	ENSG00000131381	ZFYVE20
323	YY1	hsa-miR-125b	ENSG00000007968	E2F2
324	YY1	hsa-miR-125b	ENSG00000110274	CEP164
325	YY1	hsa-miR-125b	ENSG00000119541	VPS4B
326	YY1	hsa-miR-125b	ENSG00000120656	TAF12
327	YY1	hsa-miR-125b	ENSG00000138111	TMEM180
328	YY1	hsa-miR-100	ENSG00000106348	IMPDH1
329	YY1	hsa-miR-100	ENSG00000118689	FOXO3A

Complete list of the 329 putative FFLs derived from the association of the 474 miRNA-mediated FFLs, obtained using CircuitsDB, with the available miRNA and mRNA time series data.

Additional information about the bioinformatic pipeline for mixed TF / miRNA FFLs generation

For protein-coding genes, we selected as promoter a region corresponding to (-900/+100) nts around the Transcription Start Site (TSS) of the longest transcript of each gene, being the TSS at position +1. For miRNA genes, we first grouped pre-miRNAs in the so called Transcriptional Units (TUs) (Landgraf, et al., 2007) and associated the promoter of the most 5'-upstream member of the TU to all the pre-miRNAs belonging to it. We then divided pre-miRNAs, according to their genomic annotations in inter- or intra-genic ones. Stemming from previous observations concerning miRNA regulation, see e.g. (Saini, et al., 2007; Fazi, et al., 2005; Laneve, et al., 2010), for inter-genic pre-

miRNAs we defined as putative promoter a genomic region corresponding to (-900/+100) nts upstream of the first pre-miRNA in the TU. The same definition was applied to intra-genic pre-miRNAs which showed opposite orientation with respect to the hosting protein-coding gene. Eventually, if the pre-miRNAs were intra-genic but sharing the same orientation of the hosting protein-coding gene, we associated to them as promoter region the same defined for the protein-coding host gene. The complete bioinformatic pipeline is described in (Re, et al., 2009).

References

Estelles, A., Dalmau, J., Falco, C., et al. 2001. Plasma PAI-1 levels in obese children--effect of weight loss and influence of PAI-1 promoter 4G/5G genotype. *Thromb. Haemost.* 86, 647-652.

Fazi, F., Rosa, A., Fatica, A., et al. 2005. A minicircuitry comprised of microRNA-223 and transcription factors NFI-A and C/EBPalpha regulates human granulopoiesis. *Cell* 123, 819-831.

Festa, A., D'Agostino, R.,Jr, Tracy, R.P., et al. 2002. Elevated levels of acute-phase proteins and plasminogen activator inhibitor-1 predict the development of type 2 diabetes: the insulin resistance atherosclerosis study. *Diabetes* 51, 1131-1137.

Freytag, S.O., and Geddes, T.J. 1992. Reciprocal regulation of adipogenesis by Myc and C/EBP alpha. *Science* 256, 379-382.

He, A., Zhu, L., Gupta, N., et al. 2007. Overexpression of micro ribonucleic acid 29, highly up-regulated in diabetic rats, leads to insulin resistance in 3T3-L1 adipocytes. *Mol. Endocrinol.* 21, 2785-2794.

Heine, P.A., Taylor, J.A., Iwamoto, G.A., et al. 2000. Increased adipose tissue in male and female estrogen receptor-alpha knockout mice. *Proc. Natl. Acad. Sci. U. S. A.* 97, 12729-12734.

Karbiener, M., Fischer, C., Nowitsch, S., et al. 2009. microRNA miR-27b impairs human adipocyte differentiation and targets PPARgamma. *Biochem. Biophys. Res. Commun.* 390, 247-251.

Kulshreshtha, R., Ferracin, M., Wojcik, S.E., et al. 2007. A microRNA signature of hypoxia. *Mol. Cell. Biol.* 27, 1859-1867.

Landgraf, P., Rusu, M., Sheridan, R., et al. 2007. A mammalian microRNA expression atlas based on small RNA library sequencing. *Cell* 129, 1401-1414.

Laneve, P., Gioia, U., Andriotto, A., et al. 2010. A minicircuitry involving REST and CREB controls miR-9-2 expression during human neuronal differentiation. *Nucleic Acids Res.* 38, 6895-6905.

Lee, J., Padhye, A., Sharma, A., et al. 2010. A pathway involving farnesoid X receptor and small heterodimer partner positively regulates hepatic sirtuin 1 levels via microRNA-34a inhibition. *J. Biol. Chem.* 285, 12604-12611.

Lovis, P., Roggli, E., Laybutt, D.R., et al. 2008. Alterations in microRNA expression contribute to fatty acid-induced pancreatic beta-cell dysfunction. *Diabetes* 57, 2728-2736.

Morange, P.E., Alessi, M.C., Verdier, M., et al. 1999. PAI-1 produced ex vivo by human adipose tissue is relevant to PAI-1 blood level. *Arterioscler. Thromb. Vasc. Biol.* 19, 1361-1365.

Patel, N., Tahara, S.M., Malik, P., et al. 2010. Involvement of miR-30c and miR-301a in immediate induction of plasminogen activator inhibitor-1 by placenta growth factor in human pulmonary endothelial cells. *Biochem. J.*

Re, A., Cora, D., Taverna, D., et al. 2009. Genome-wide survey of microRNA-transcription factor feed-forward regulatory circuits in human. *Mol. Biosyst* 5, 854-867.

Regazzetti, C., Peraldi, P., Gremeaux, T., et al. 2009. Hypoxia decreases insulin signaling pathways in adipocytes. *Diabetes* 58, 95-103.

Rodriguez-Gonzalez, F.G., Sieuwerts, A.M., Smid, M., et al. 2010. MicroRNA-30c expression level is an independent predictor of clinical benefit of endocrine therapy in advanced estrogen receptor positive breast cancer. *Breast Cancer Res. Treat.*

Saini, H.K., Griffiths-Jones, S., and Enright, A.J. 2007. Genomic analysis of human microRNA transcripts. *Proc. Natl. Acad. Sci. U. S. A.* 104, 17719-17724.

Sun, T., Fu, M., Bookout, A.L., et al. 2009. MicroRNA let-7 regulates 3T3-L1 adipogenesis. *Mol. Endocrinol.* 23, 925-931.

Yun, Z., Maecker, H.L., Johnson, R.S., et al. 2002. Inhibition of PPAR gamma 2 gene expression by the HIF-1-regulated gene DEC1/Stra13: a mechanism for regulation of adipogenesis by hypoxia. *Dev. Cell.* 2, 331-341.